

**GAMMA-RAY ALBEDO OF SMALL SOLAR SYSTEM BODIES.** I. V. Moskalenko<sup>1,2</sup>, T. A. Porter<sup>3</sup>, S. W. Digel<sup>2,4</sup>, P. F. Michelson<sup>1,2</sup>, and J. F. Ormes<sup>5</sup>, <sup>1</sup>Hansen Experimental Physics Laboratory, Stanford University, Stanford, CA 94305 ([imos@stanford.edu](mailto:imos@stanford.edu)), <sup>2</sup>Kavli Institute for Particle Astrophysics and Cosmology, Stanford University, Stanford, CA 94309, <sup>3</sup>Santa Cruz Institute for Particle Physics, University of California, Santa Cruz, CA 95064, <sup>4</sup>Stanford Linear Accelerator Center, 2575 Sand Hill Road, Menlo Park, CA 94025, <sup>5</sup>Department of Physics and Astronomy, University of Denver, Denver, CO 80208.

**Introduction:** We calculate the  $\gamma$ -ray albedo flux from cosmic-ray (CR) interactions with the solid rock and ice in Main Belt asteroids and Kuiper Belt objects (KBOs) using the Moon as a template. We show that the  $\gamma$ -ray albedo for the Main Belt and KBOs strongly depends on the small-body mass spectrum of each system and may be detectable by the forthcoming *Gamma Ray Large Area Space Telescope* (GLAST). If detected, it can be used to derive the mass spectrum of small bodies in the Main Belt and Kuiper Belt and to probe the spectrum of CR nuclei at close-to-interstellar conditions. The orbits of the Main Belt asteroids and KBOs are distributed near the ecliptic, which passes through the Galactic center and high Galactic latitudes. Therefore, the  $\gamma$ -ray emission by the Main Belt and Kuiper Belt has to be taken into account when analyzing weak  $\gamma$ -ray sources close to the ecliptic. The asteroid albedo spectrum also exhibits a 511 keV line due to secondary positrons annihilating in the rock. This may be an important and previously unrecognized celestial foreground for the *INTErnational Gamma-Ray Astrophysics Laboratory* (INTEGRAL) observations of the Galactic 511 keV line emission including the direction of the Galactic center. For details of our calculations and references see [1].

**Small Solar System Bodies (SSSB):** The populations of SSSB in the asteroid belt between Mars and Jupiter and in the Kuiper Belt beyond Neptune's orbit remain the least explored members of the solar system. A majority of asteroids in the Main Belt have their orbits close to the ecliptic while the Kuiper Belt has a wide distribution in ecliptic latitude with an angular area  $8100^{+1500-1100}$  deg<sup>2</sup> and a FWHM of  $12.5^\circ \pm 3.5^\circ$  in ecliptic latitude [2]. The asteroid mass and size distributions are usually assumed to obey power laws:  $dN = am^{-k}dm$ ,  $dN = br^{-n}dr$ , where  $m$  is the asteroid mass,  $r$  is the asteroid radius, and  $a$ ,  $b$ ,  $k$ ,  $n$  are constants. Assuming all bodies have the same density  $\rho$ , one can derive  $n = 3k-2$  and  $b = 3a(4\pi\rho/3)^{1-k}$ . The number of the Main-Belt asteroids larger than diameter  $D$  (in km) is  $N(>D) = 1.9 \cdot 10^6 D^{-2.52}$  [3]; a similar distribution  $dN(r)/dr \sim r^{-3.5}$  is obtained based on a theoretical collisional model of fragmentation [4]. Observations with *Infrared Space Observatory* (ISO) [5] give  $\log N(>D) = (5.9324$

$\pm 0.0016) - (1.5021 \pm 0.045) \log D$  for  $0.2 \text{ km} < D < 2 \text{ km}$ .

The densities of most asteroids lie in the range  $1.0 - 3.5 \text{ g cm}^{-3}$  [3] while the densities of particular asteroid classes can vary broadly,  $1.23 - 1.40 \text{ g cm}^{-3}$  for carbonaceous,  $2.65 - 2.75 \text{ g cm}^{-3}$  for silicate, and  $4.75 - 5.82 \text{ g cm}^{-3}$  for metallic bodies [4]. Most of the asteroids in the Main Belt have circular orbits with radius  $\ell \sim 2.5 \text{ AU}$ . The dynamical estimate of the total mass of the asteroid belt is about  $(3.6 \pm 0.4) \cdot 10^{24} \text{ g}$  [4] or close to 5% of the mass of the Moon.

The Kuiper Belt (and the innermost part of the Oort Cloud) is further away than the asteroid belt; its objects are distributed between 30–100 AU [6] with surface number density  $\sigma(\ell) = A\ell^{-\alpha}$  [6,7], where  $A$  is a constant, and  $\alpha = 2$ . The total mass is  $\sim 0.3M_{\text{Earth}}$  ( $1.8 \cdot 10^{27} \text{ g}$ ), where  $M_{\text{Earth}}$  is the Earth mass. The density of small icy bodies and comets is  $0.5 \text{ g cm}^{-3}$  [8,9]. The size distribution is described by a power law with  $n = -3.5$ .

**Results:** We use the Lunar albedo spectrum as an approximation of the SSSB albedo for two main reasons: (i) the Moon is a solid body in which the CR cascade in the rock develops similarly, and (ii) its proximity to the Earth allows it to be easily detectable by  $\gamma$ -ray telescopes. The flux of  $\gamma$ -rays from the Moon  $F_{\text{Moon}}$  has been calculated recently [1,10] using the GEANT4 Monte Carlo framework to simulate the CR cascade development in a Lunar rock target (regolith) and is in agreement with observations [11].

For the Main Belt we use the following parameters:  $\rho = 2 \text{ g cm}^{-3}$  is the average density of the asteroids (regolith), the largest asteroid size  $r_1 = 4.565 \cdot 10^7 \text{ cm}$  (dwarf planet Ceres),  $r_0 = 100 \text{ cm}$  is the smallest radius of an asteroid that is still an opaque target for incident CR. For these parameters, the total asteroid albedo flux is  $F_{\text{tot}}/F_{\text{Moon}} = 0.003, 0.81, 183$  for  $n = 2.5, 3.0, 3.5$ , correspondingly. The removal of Ceres, which is  $\sim 30\%$  of the total mass of the asteroid belt alone, from the calculation does not change the result much.

The Kuiper Belt is further away than the Main Belt, but is much more massive. The second largest dwarf planet of the Kuiper Belt after Eris is Pluto  $r_1 = 1.2 \cdot 10^8 \text{ cm}$ , while the majority of the Kuiper Belt objects are icy rocks and comets with  $\rho = 0.5 \text{ g cm}^{-3}$ . The total Kuiper Belt albedo flux is about the same as of the

Main Belt assuming the same incident CR flux. However, the incident spectrum of CR particles at  $>30$  AU approaches the local interstellar spectrum which results in a factor of  $\sim 2$  increase below  $\sim 1$  GeV. For these parameters, the total Kuiper Belt albedo flux is  $F_{\text{tot}}^{\text{K}}/F_{\text{Moon}} = 0.006, 2.25, 820$  for  $n = 2.5, 3.0, 3.5$ , correspondingly.

Our estimates and the analysis of the EGRET data (Fig.1) show that the integral flux of the KBO and the Main Belt is  $< 6 \cdot 10^{-6} \text{ cm}^{-2} \text{ s}^{-1}$  (100–500 MeV), i.e.  $< 12F_{\text{Moon}}$ , which implies that the value of  $n$  should be close to 3. The detection of the CR-induced albedo of the Main Belt asteroids and the KBOs by GLAST is possible. At higher energies  $> 1$  GeV where the  $\gamma$ -ray albedo flux is steady and does not depend on the solar modulation, it can serve as a normalization point to the cumulative brightness of all asteroids plus the Kuiper Belt. At lower energies  $< 1$  GeV, the Kuiper Belt albedo dominates and the albedo will tell us directly about the LIS spectrum of CRs. Therefore, the observations of the albedo flux can provide us with valuable information about the size distributions of SSSBs in both regions, while the shape of the albedo spectrum can tell us about the LIS spectra of CR protons and helium at high energies. In turn, a detection of the asteroid belt and the Kuiper Belt albedo at MeV-GeV energies will enable us to normalize properly the cumulative albedo spectrum and make a prediction for the intensity of the 511 keV line.

Our estimates of the fluxes assume that the mass and radius distributions are valid for the whole range of masses, which is not necessarily true. We also assumed spherical bodies. However, the smallest bodies are distinctly non-spherical which would make them somewhat brighter than we have estimated. Thus, our calculations underestimate the SSSB albedo emission.

The GLAST Large Area Telescope (LAT) (<http://glast.stanford.edu>), to be launched by NASA in 2008, will in just a year of surveying the sky have exposures a factor of 40 or more deeper than EGRET and will be free from sensitivity variations owing to ageing of consumables. This capability will permit detection of albedo  $\gamma$ -ray fluxes for SSSBs at even the Lunar flux level.

**References:** [1] Moskalenko I. V. et al. (2008) *ApJ submitted*, arXiv:0712.2015. [2] Brown M. E. (2001) *AJ*, 121, 2804. [3] Binzel R. P. et al. (1999) in *Allen's Astrophysical Quantities*, 315. [4] Krasinsky G. A. et al. (2002) *Icarus*, 158, 98. [5] Tedesco E. F. and Desert F.-X. (2002) *AJ*, 123, 2070. [6] Backman D. E. et al. (1995) *ApJ*, 450, L35. [7] Jewitt D. C. and Luu J.-X. (1995) *AJ*, 109, 1867. [8] Asphaug E. and Benz W. (1994) *Nature*, 370, 120. [9] Solem J. C. (1994)

*Nature*, 370, 349. [10] Moskalenko I. V. and Porter T. A. (2007) *ApJ*, 670, 1467. [11] Thompson D. J. et al. (1997) *JGR*, A120, 14735. [12] Hartman R. C. (1999) *ApJS*, 123, 79. [13] Sowards-Emmerd D. et al. (2003) *ApJ*, 590, 109. [14] Sowards-Emmerd D. et al. (2004) *ApJ*, 609, 564.

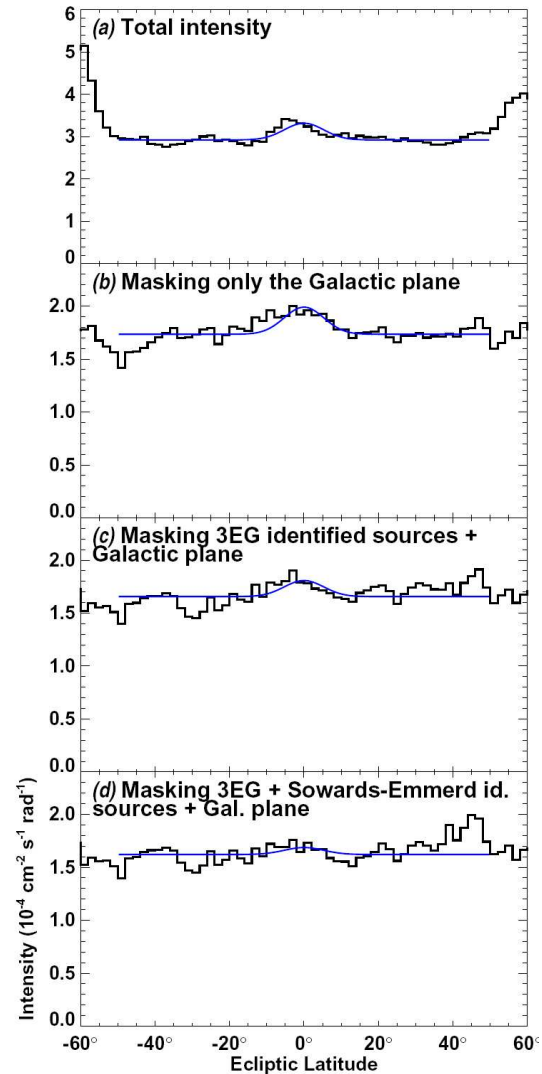


Fig.1. Profiles of  $\gamma$ -ray intensity with  $\beta$  (ecliptic latitude) derived from EGRET data. The energy range is 100 – 500 MeV and the profiles have been averaged over all ecliptic longitudes. (a) Profile derived with no masking of Galactic diffuse emission or  $\gamma$ -ray point sources. (b) Profile with the Galactic plane ( $|b| < 10^\circ$  for  $||| > 90^\circ$  and  $|b| < 20^\circ$  for  $||| < 90^\circ$ ) excluded. (c) Profile with the identified 3EG sources [12] and the Galactic plane excluded. (d) Profile with the identified 3EG sources plus the further blazar identifications proposed by [13,14] excluded. Overlaid on each profile is the best-fitting Gaussian ( $12.5^\circ$  FWHM, centered on  $\beta = 0$ ) plus a constant, fit for the region  $\beta < 50^\circ$ .